scientific reports

Check for updates

OPEN

Anticancer, antimicrobial and antioxidant activity of CuO–ZnO bimetallic nanoparticles: green synthesised from *Eryngium foetidum* leaf extract

Jennifer Daimari & Anamika Kalita Deka ✉

In the present study, green synthetic pathway was adapted to synthesize CuO–ZnO bimetallic nanoparticles (BNPs) using *Eryngium foetidum* leaf extract and their anti-cancer activity against MCF7 breast cancer cell lines, anti-microbial activity and in vitro anti-oxidant activity were evaluated. Various bio-active compounds present in leaf extract were responsible for the reduction of CuO–ZnO NPs from respective Cu^{2+} and Zn^{2+} metal precursors. In the present study, the involvement of bio-active compounds present in *E. foetidum* extract before and after green synthesis of BNPs were evaluated for the first time. Rod-shaped and spherical structural morphology of synthesized BNPs were revealed by using FESEM, TEM, and XRD analysis with particle size ranged from 7 to 23 nm with an average size of 16.49 nm. The distribution of Cu and Zn were confirmed by elemental mapping. The green synthesized CuO–ZnO NPs showed significant cytotoxic effect with the inhibition rate 89.20 ± 0.03% at concentration of 500 µg/mL. Again, good antioxidant activity with $IC_{50;}$ 0.253 mg/mL and antimicrobial activity of BNPs were also evaluated with the increasing order of MIC; *E. coli* (7.81 µg/mL) < *B. subtilis* (62.5 µg/mL) < *S. aureus* (31.25 µg/mL).

Keywords Green synthesis, *E. foetidum*, BNPs, Antioxidant, Antimicrobial, Anticancer

Green synthesized metal nanoparticles (NPs) and metal oxide nanoparticles (MO-NPs) are having greater acceptability over traditional chemical synthesized ones because of environmentally friendly non-toxic nature as well as ecofriendly behavior[1]. Various parts of plants viz., leaves, stem, roots, fruits, peels of fruits and vegetables are generally utilized as reducing agent for the synthesis of NPs and MO-NPs. The phytocomponents present in plants like; polyphenols, flavonoids, carotenoids, terpenoids are acts as main reducing agent during green synthesis. NPs and MO-NPs are of particle size less than 100 nm; widely used in nano-bioscience and nanotechnology research recently because of their remarkable wide applications in biological, disinfectants, antimicrobial agents, drug delivery and catalytic products[2].

Over the past decade, bimetallic nanoparticles (BNPs) have been extensively researched and applied in various scientific and technological fields. BNPs are reported to exhibit greater stability compared to monometallic nanoparticles due to the synergistic interaction between the metals and are more useful due to their potential applications across various scientific and technological fields[3,4]. Based on the metal precursors and capping agents used, the BNPs exhibit improved electronic, catalytic, pharmaceutical, and optical actions[5,6]. BNPs can be synthesised by both bottom-up and top-down methods viz., biological synthesis, chemical synthesis, physical synthesis, pyrolysis and thermolysis etc., out of which biosynthesis approach has garnered significant attention due to its environmentally friendly nature. Nanoparticles synthesized through this method, using plant extracts, bacteria, or fungi, possess unique and enhanced properties, making them promising candidates for biomedical applications as nanomedicine, in particular, holds significant promise for the potential treatment of diseases

Department of Chemistry, Central Institute of Technology Kokrajhar (Deemed to be University, under MoE, Govt. of India), Kokrajhar, Assam 783370, India. ✉email: a.kalita@cit.ac.in

and advancements in diagnosis as mentioned above[7,8]. MO-NPs ZnO, TiO_2, CaO, SnO_2, CeO_2 and CuO have been investigated with various biomedical and environmental applications[1,2,9]. For instance, Arumugam et al., reported that the *Gloriosa superba* leaf extract-mediated green synthesized CeO_2-NPs with good anti-microbial activity[1,10]. Zaqri et al., reported that *Senna auriculata* flower extract mediated NiO-NPs with anti-microbial activity against *Escherichia coli* gram-negative bacteria[11]. Monometallic metal oxides ZnO and CuO, produced through environmental friendly synthetic routes, are recognized for their excellent antibacterial and biomedical applications[5,6]. Velsankar et al., reported *Echinochloa frumentacea* grain extract-mediated ZnO-NPs with hexagonal shapes and evaluated with strong antibacterial activity against *Bacillus pumilus* and *Salmonella typhi* with good cytotoxicity against *E. coli* AB1157[12]. Again, ZnO-NPs prepared from *Curcurbita* seed extract also showed anti-fungal activity against *Aspergillus flavus* and *Aspergillus niger* fungi[13]. Biosynthesized ZnO-NPs from *Paspalum scrobiculatum* grains were observed with potent drug features against $HepG_2$ liver cancer; with 97.18% cytotoxicity per 100 µg/mL concentration of ZnO-Nps[14]. Similarly, ZnO-NPs synthesized from *Erythrina variegate* leaf extract were analysed with strong inhibition against gram-negative (*Salmonella typhi*) and gram-positive (*Bacillus subtilis* and *Staphylococcus aureus*) bacteria[15].

Again, CuO nanoparticles exhibit biocidal and antimicrobial properties, making them suitable for biomedical applications with few limited toxic effects[16]. For instance, Velsankar K. et al., reported CuO NPs biosynthesized from *Plectranthus amboinicus* leaf extracts. They found strong anti-diabatic and anti-larvicidal activity with IC_{50}, 243.08 µg/mL and low LC_{50} values respectively[17]. CuO-NPs green synthesized from *Panicum sumatrense* grain extracts has been observed with anti-cancer activity against MCF-7 breast cancer cells in low IC_{50} value[18]. Strong anti-microbial, anti-fungal and anti-larvicidal activity was demonstrated by green synthesized *Allium sativum* extract mediated CuO-NPs[19]. Again, CuO-NPs synthesized from leaf-extract of *Capsicum frutescens* was observed with anti-bacterial activities against gram-positive bacteria; *Bacillus anthracis* and *Listeria monocytogenes* respectively. CuO-NPs possessed anti-bacterial activity against gram-negative bacteria *Klebsiella pneumoniae* with strong inhibition at concentrations ranged from 92 to 150 µg/mL concentration of CuO-Nps[20].

On the other hand, ZnO nanoparticles are less toxic and cost-effective, making them excellent for biomedical applications compared to other metals[21]. Again, the bimetallic nanoparticles CuO–ZnO NPs have been reported to demonstrate strong cytotoxicity, antioxidant and antimicrobial activities, further highlighting their potential in various therapeutic remedies[22].

The *E. foetidum* plant, a member of the *Apiaceae* family, is widely distributed across different continents and is used both as an herb and in culinary practices[23]. The entire plant is strongly fragrant and smooth. Phytochemical analysis has revealed the presence of essential oils, including *E*-2-dodecenal or "eryngial," in its leaves[24]. Traditionally, *Eryngium foetidum* has been used in Asia and Latin America as ethnomedicine, often brewed as a tea to treat stomach pains[25]. In North-Eastern India, it is consumed as a spice, in salads, and as a side dish. Extracts from this plant have shown promising biomedical applications, acting as anti-inflammatory, antibacterial, and antimalarial agents[23].

Currently, cancer is a major cause of death, with an estimated 18.1 million new cases and 9.6 million deaths in 2018 alone. Among these cases, female breast cancer accounts for 11.6%, making it the most common cancer among women[26]. Biosynthesized nanoparticles offer a new approach to cancer therapy. Nanoparticles derived from plant extracts can stimulate cellular growth and halt the cell cycle in cancerous cells[27]. One of the main factors affecting cancer cells is the production and excretion of oxygen free radicals, which are normally present in low levels in the body. However, when produced in large quantities, these radicals can react with other molecules in the body where the antioxidants in the body help to neutralize free radicals[28].

Naturally occurring antioxidants are primarily sourced from plants. Phenolics, vitamins, microelements, and carotenoids are commonly found in green vegetables, herbs, fruits, and spices[29]. Reactive oxygen species (ROS) such as hydroxyl radical (·OH), hydrogen peroxide (H_2O_2), superoxide anion ($\cdot O_2^-$) and singlet oxygen ($^1O_2$) are generated as a result of natural oxidative stress, arising from electronic excitation or redox reactions[30]. This oxidative stress plays a significant role in various common diseases, including high blood pressure, diabetes, Alzheimer's, preeclampsia, and Parkinson's disease[31,32]. Elevated levels of ROS within cells can greatly impact cell function, leading to diseases and cellular deficiencies. Antioxidant compounds obtained from food or diet can be present in the human body in very small concentrations, yet they can effectively delay or prevent oxidative processes that contribute to disease development[32,33]. Biosynthesized metal nanoparticles, BNPs can serve as antioxidants by interacting with reactive oxygen species (ROS) to reduce oxidative stress.

Bacterial and microbial infections are significant causes of mortality and chronic illnesses[34]. Nanoparticles offer a promising solution by effectively combating microbial drug resistance in some cases[35]. They interact with microbial cell membranes, inhibiting microbes and preventing resistance[36]. Functional nanomaterials have been studied for their potential in accelerating wound healing and enhancing bone implant effectiveness[36]. Therefore, nanoparticles are increasingly seen as an excellent alternative to antibiotics, capable of developing multidrug resistance against pathogens[35]. Various types of nanoparticles, such as BNPs, Au–Ag, Au-ZnO, and Ag-ZnO, exhibit antimicrobial activity by damaging microbial DNA and proteins, inducing oxidative stress, and disrupting microbial membranes[37]. For instance, BNPs Se/Zr prepared from *Cinnamomum camphora* leaf extract was reported with anti-cancer activity against breast cancer cell line[38]. ZnO-CuO hexagonal shaped BNPs green synthesized from *Sambucus nigra* L. extract was reported with anti-cancer activity against lung and human melanoma cell lines[39]. Medeshwaran et al., reported bio-synthesized ZnO-CuO spherical BNPs with bacteria-fighting ability and strong anti-cancer activity MCF-7 cell line[40].

The present study investigated the therapeutic potential of CuO–ZnO bimetallic nanoparticles synthesized from *Eryngium foetidum* extracts for first time. The BNPs were evaluated for their antimicrobial activity against *Escherichia coli*, *Enterobacter aerogenes*, *Staphylococcus aureus*, and *Bacillus subtilis*. Additionally, their anticancer properties were studied on the MCF7 breast cancer cell line, and antioxidant activity was assessed using the DPPH assay.

Experimental

Reagents and plant collection

Copper (II) chloride dihydrate [$CuCl_2 \cdot 2H_2O$] and zinc nitrate hexahydrate [$Zn(NO_3)_2 \cdot 6H_2O$], with purities of 98.5% and 96%, respectively, were procured from Merck Life Science Pvt. Limited in Mumbai, India. 2,2-diphenylpicrylhydrazyl (DPPH, purity 95%) and methanol were obtained from SRL Chemical in Mumbai, India. Sodium hydroxide pellets were sourced from Finar Chemicals Limited in Ahmedabad, India. Nutrient broth, Mueller Hinton agar (MHA), DMEM medium, and MTT Reagent media were acquired from HiMedia in Mumbai, India, while sodium chloride was obtained from Merck Emplura in Mumbai, India. The MCF7-Human Breast cancer cell line was purchased from the National Centre for Cell Science, Pune, India. The Standard Cisplatin was procured from Sigma Aldrich. Analytical-grade reagents were utilized in the study without undergoing additional purification. The primary solvent employed was double deionized distilled water (DDW).

Eryngium foetidum L., commonly known as "*Culantro*" or "*Gongar dundiya*" in the *Bodo* language, was gathered from the Kokrajhar district of Assam in North-East India. Subsequently, the leaves underwent oven-drying then powdered and were stored in an airtight container for future use.

Preparation of the extract

The harvested *Eryngium foetidum* leaves underwent a thorough washing with distilled water, followed by drying in an oven at 50 °C and grinding into a fine powder using a mortar. This powder was then utilized in the preparation of an aqueous plant extract. The extraction process involved a ratio of 5:1 (v/w) of distilled water to plant extract, where approximately 2 g of *E. foetidum* leaf powder was combined with 100 mL of DDW and boiled for 10 min. Subsequently, the mixture underwent filtration using Whatman Filter paper no. 44, and the resulting filtrate was stored in a refrigerator at 4 °C for future use. This extract served the dual purpose of functioning as both reducing and stabilizing agents.

Synthesis of bimetallic CuO–ZnO nanoparticles

To synthesize bimetallic nanoparticles (CuO–ZnO) or BNPs a solution was prepared by transferring 0.1 M of copper chloride dihydrate and 0.1 M zinc nitrate hexahydrate into a 250 mL conical flask containing 100 mL of double-distilled water (DDW). Subsequently, 50 mL of *E. foetidum* extract was slowly added to the mixture. The resulting solution underwent continuous stirring on a magnetic stirrer at 60 °C for a duration of 3 h, during which the solution's colour transitioned from light blue to dark green and then to deep blue. After this process, the solution was subjected to centrifugation at 2500 rpm using a REMI centrifuge with a REMI R-8C rotor for 15 min at room temperature, and the resultant mixture was collected. The collected mixture was then subjected to drying and calcination at 400 °C to yield bimetallic (CuO–ZnO) nanoparticles.

Characterization of synthesized CuO–ZnO nanoparticles

The UV–visible Spectroscopy analysis of CuO–ZnO nanoparticles (BNPs) was conducted using UV-2600, Shimadzu, Japan. Fourier-transform infrared spectroscopy (Shimadzu IR Affinity–1S, Japan) was employed to investigate the surface composition. The X-ray diffraction analysis of BNPs was performed using the D8 Advance instrument from Bruker to examine their crystallinity. The morphology and size of BNPs were examined through Field Emission Scanning Electron Microscopy (SIGMA VP, Zeiss) and Transmission Electron Microscopy (JEOL, 200 kV, Model No. JEE–2100).

Bioanalytical analysis by high performance liquid chromatography

The phytochemical constituents were specified using reverse phase High Performance Liquid Chromatography with Diode Array Detector (DAD).The HPLC (Agilent Technologies 1260 infinity Series) instrument was equipped with Quaternary pump 1260 Quat. Pump VL, 1260 ALS Autosampler, 1260 TCC column oven, a Zorbax Eclipse Plus C18 column (250 mm, 4.6 mm i.d, 5 µm) and a 1260 DAD VL+ detector. All the components of the chromatographic system were controlled using Open Lab CDS EZ Chrom system controller. Data acquisition was performed by using Open Lab CDS Data Analysis ver. A.01.01 software. The chromatographic analysis was performed on reverse-phase Zorbax Eclipse Plus C18 column with the flow rate of 1.2 mL/min and temperature at 20 °C ± 1. Diode array detection was carried out at various wavelength of 270, 280, 310, 320 and 370 nm respectively.

Antioxidant activity

To assess the antioxidant activity of BNPs, DPPH (1,1-diphenyl-2-picrylhydrazyl) was employed. A 0.1 mM DPPH stock solution was prepared in 0.1 L of methanol and added to varying concentrations (0.1, 0.3, 0.5, 0.7, 0.9 and 1 mL) of BNPs, with chlorogenic acid (CGA) as the reference. The mixture underwent a 30 min incubation in a dark environment at 30 °C. Subsequently, absorption at 517 nm was measured using a UV–vis spectrophotometer. To calculate the percentage inhibition for scavenging activity, the subsequent formula was applied.

$$\text{DPPH Scavenging activity (\%)} = \left(\text{Abs of control} - \text{Abs of sample/Abs of control}\right) \times 100 \quad (1)$$

The IC_{50} value was determined using varying concentrations of the sample under investigation.

Antimicrobial activity

Well diffusion assay

The antimicrobial activity of BNPs against *Escherichia coli* (ATCC 25922), *Enterobacter aerogens* (ATCC 13048), *Staphylococcus aureus* (ATCC 23235) and *Bacillus subtilis* (ATCC 6051a) were assessed using the agar well

diffusion method. For each bacterial strain, a subculture of 200 µL, equivalent to 10^6 CFU/mL, was evenly spread on a nutrient agar petri dish (20 mL) using a sterile cotton swab. Wells with an 8 mm diameter were created using a sterile gel borer, and four wells were designated for each bacterial strain. BNPs dissolved in concentrations of 1 mg/mL, 2 mg/mL, and 3 mg/mL were used, with each well containing 100 µL of BNPs. The plates were then incubated at 37 °C for 24 h, and the measurement of the zone of inhibition around the wells were conducted after the incubation period.

Minimum inhibitory concentration (MIC)
The Minimum Inhibitory Concentrations (MICs) of BNPs against *Escherichia coli* (ATCC 25922), *Enterobacter aerogens* (ATCC 13048), *Staphylococcus aureus* (ATCC 23235) and *Bacillus subtilis* (ATCC 6051a) were determined using the broth dilution method. The test compound was dissolved in Dimethyl sulfoxide (DMSO), and prepared at various concentrations (1 mg/mL, 2 mg/mL, and 3 mg/mL). Ampicillin was employed as a positive control, while DMSO served as the negative control. Standardized microbial suspensions were inoculated and incubated for 16–18 h at 37 °C to establish fresh cultures. In test tubes containing 5 mL of nutrient media, 100 µL of the test concentrations (1 mg/mL, 2 mg/mL, and 3 mg/mL) were added. Additionally, 20 µl of the fresh microbial cultures were inoculated into all the tubes. Following a 20 h incubation at 37 °C, the tubes were examined for turbidity.

Minimum bactericidal concentration (MBC)
Escherichia coli (ATCC 25922), *Enterobacter aerogens* (ATCC 13048), *Staphylococcus aureus* (ATCC 23235) and *Bacillus subtilis* (ATCC 6051a) were chosen to determine the Minimum Bactericidal Concentration (MBC) of a prepared sample of BNPs. The MIC concentration and its higher counterpart for each microbial strain were assessed for MBC. Individual LB agar plates were used for spreading and drying each microbial strain. Subsequently, 100 µL of the afore mentioned concentrations were spread on the plates and incubated for 20 h at 37 °C. The petri plates were then examined for the presence of bacterial colonies. LB agar plates with organisms, along with ampicillin, were employed as positive controls.

Time kill assay
Time kill assay followed the MIC and MBC assessments, tracking changes in microbial growth over 24 h intervals. The experiment was carried out in test tubes under conditions similar to those used for MIC, with incubation at 37 °C. After 24 h period, a 100 µL sample was withdrawn from the culture for determination of CFU/mL using the plate count technique. Following a subsequent 24 h incubation at 37 °C, newly formed microbial colonies were enumerated and CFU/mL values calculated. The results were compared with the count from the culture control lacking the BNPs.

Cytotoxicity evaluation (MTT assay) against MCF7 cell line

The MCF7 human breast cancer cell line was seeded into individual wells of 96-well plates (Corning, USA) at a concentration of 20,000 cells per well, using 200 µl of cell suspension. The plates were then incubated overnight. Subsequently, varying concentrations of BNPs (25 µg, 50 µg, 100 µg, 250 µg, and 500 µg) were introduced, and the plates were further incubated for 24 h at 37 °C in a 5% CO_2 atmosphere (Heal force, China). Following the incubation period, MTT reagent was added, and the plates were placed back in the incubator for 3 h in the absence of light. After this incubation, the MTT reagent's supernatant was aspirated, and 100 µl of DMSO was added to dilute the formed purple-blue colour. The absorbance was then measured at 570 nm using a spectrophotometer or ELISA reader (ELX-800, BioTek, USA)[41,42]. Cell viability was calculated using the subsequent formula.

$$\text{Cell viability (\%)} = \left(\text{OD of treated sample/OD value of untreated cells}\right) \times 100 \quad (2)$$

The IC_{50} value was also determined.

Statistical analysis

All experiments were conducted in triplicate and the reported results represent the averages of these trials. The statistical analysis was done by using one-way ANOVA in Microsoft Excel 2021. *P*-values of $\alpha = 0.05$ were deemed statistically significant.

Results

Characterization on CuO–ZnO NPs

The optical characterization of green synthesized BNPs were done by UV–visible spectroscopy. The UV–visible spectrum of CuO–ZnO nanoparticles exhibited a wide-ranging spectrum from 230 to 530 nm. The peak wavelength (λ_{max}) observed in this spectrum was 344 nm. The UV–visible spectrum of BNPs is shown in Fig. 1. The appearance of no other peaks in the UV–Vis spectrum confirmed the absence of Cu/Zn nanoparticle agglomeration or very little agglomeration[43].

Figure 2 shows the FTIR of both the plant extract and synthesized BNPs. In the plant extract, characteristic bands were observed at 3310, 2907, 2358, 2331, 1732, 1631, 1421, and 1064 cm^{-1}. The band at 3310 cm^{-1} indicated the -OH stretching of plant polyphenols, while the band at 2907 cm^{-1} was associated with the stretching vibrations of CH, CH_2, and CH_3 groups found in carbohydrates, flavonoids, and polyphenols[44,45]. The presence of ester carbonyl (C=O) groups and carboxylate ions (COO–) was revealed by peaks at 1732 and 1631 cm^{-1}, respectively[46]. The band at 1421 cm^{-1} was attributed to the C=C stretching vibration of aromatic polyphenols

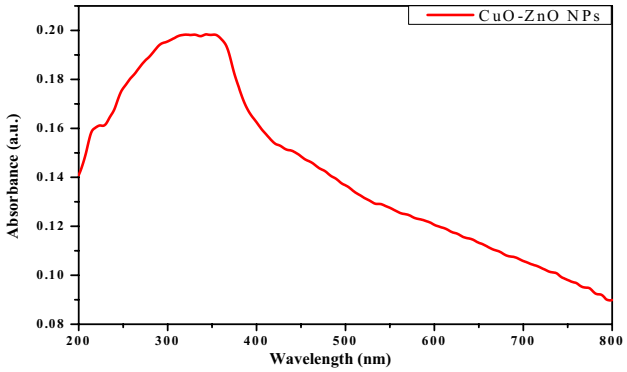

Figure 1. UV–visible absorption spectra of *E. foetidum* synthesized CuO–ZnO NPs.

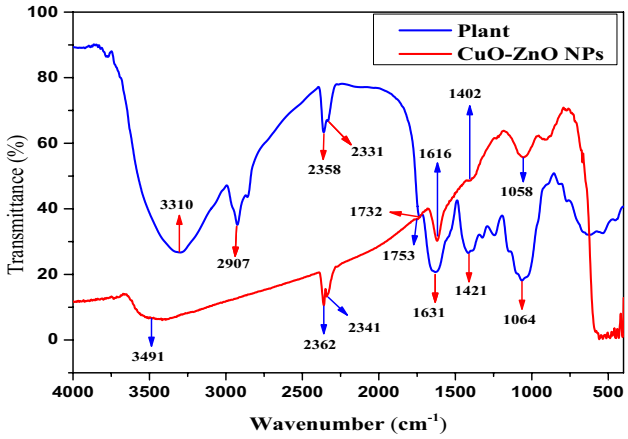

Figure 2. FTIR spectra of *E. foetidum* synthesized CuO–ZnO NPs.

containing phenyl rings, and the band at 1064 cm^{-1} was linked to the C–OH group of phenols, indicating the presence of bio-reducing agents such as flavonoids and terpenoids[47,48].

The FTIR spectrum of the BNPs displayed bands at 3491, 2362, 2341, 1616, 1402, and 1058 cm^{-1}. A comparison of the frequencies of these bands with those of the plant extract revealed shifts from 3491, 2362, 2341, 1753, 1616, 1402, and 1058 cm^{-1} for BNPs to 3310, 2907, 2358, 2331, 1732, 1631, 1421, and 1064 cm^{-1} for the plant extract. This shift indicated that the functional groups in the plant extract acted as reducing agents during the synthesis of BNPs, leading to modifications in the FTIR spectrum. The presence of these functional groups contributed to the reduction and stabilization processes involved in the synthesis of CuO–ZnO NPs[49,50]. The reduction of metal precursors to BNPs might be due to functional groups containing molecules like flavonoids, polyphenols etc.

Figure 3 shows the XRD crystalline pattern of CuO–ZnO BNPs. Distinct peaks were identified at 2θ values of 31.7, 34.4, 36.1, 47.6, 56.5, 62.8, and 67.9° in the X-ray diffraction pattern analysis. These values validated the existence of planes (100), (002), (101), (102), (110), (103), and (112), respectively. These results are in agreement with the JCPDS card 01-080-0075[39] which describes the hexagonal phase and crystalline structure of ZnO NPs. Furthermore, according to JCPDS card 01-080-1917[51], peaks at 2θ values of 35.4, 38.6, 48.4, and 66.2° correspond to planes (111), (200), (202), and (310), respectively, demonstrating the crystal structure and monoclinic phase of CuO NPs. The average crystalline size of green synthesized CuO–ZnO NPs were calculated using Debye- Scherrer's equation; ranged between 7 to 23 nm. The peak intensities for ZnO-NPs were higher than CuO-NPs. ZnO have higher percentage and crystallinity than CuO. The low peak intensity and crystallinity of CuO may be due to the coating role of ZnO-NPs on them[39,52].

FESEM surface morphology and EDX measurements of CuO–ZnO BNPs are shown in Fig. 4**.** Rod-shaped structures with a polygonal design were observed for CuO–ZnO BNPs (Fig. 4A,B). Figure 4B also demonstrated the presence of isometric NPs ranging in size from 50 to 200 nm, showcasing the variety of shapes. The purity of the synthesized BNPs was confirmed by EDX investigation (Fig. 4C). The weight percentage of of Zn, Cu, and O—atoms observed were 34.28%, 30.12%, and 25.06%, respectively. The synthesized BNPs were isometric NPs in the 50–200 nm range and unique rod-shaped structures. The detection of carbon from the plant extract underscored the green synthesis technique and emphasized the effect of natural ingredients on the final composition.

Transmission Electron Microscopy (TEM) was employed to assess the size of BNPs. The results showed that the CuO–ZnO NPs were mostly rod shaped with some spherical shaped particles (Fig. 5A,B). This is due to

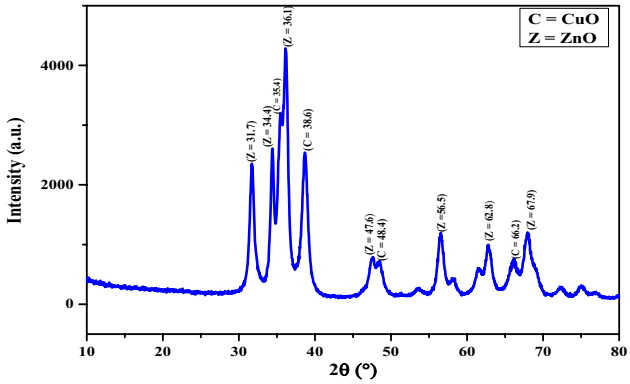

Figure 3. XRD pattern of *E. foetidum* synthesized CuO–ZnO NPs.

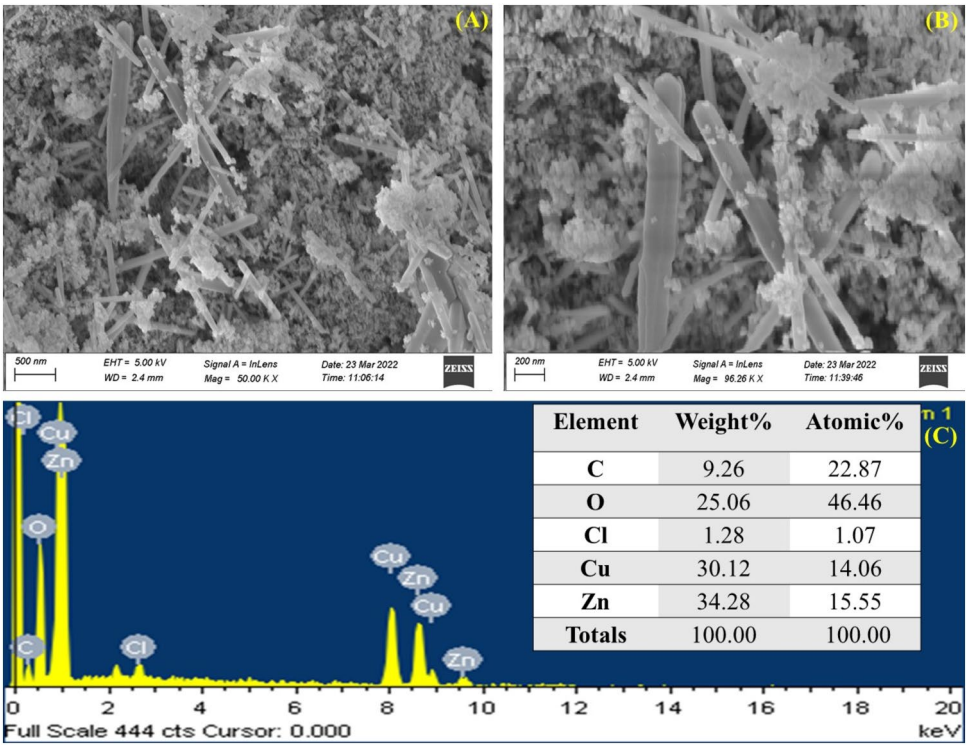

Figure 4. (**A**) and (**B**) FESEM images and (**C**) EDX spectra of *E. foetidum* synthesized CuO–ZnO NPs.

agglomeration of some NPs. The particle size was precisely determined, yielding an average size of 16.49 nm. To further examine the crystalline morphology of the BNPs, selected area electron diffraction (SAED) patterns were employed (Fig. 5C). These patterns revealed a well-defined crystalline structure of the NPs, supporting our findings from the TEM analysis.

Elemental mapping of BNPs as shown in Fig. 6 revealed that ZnO and CuO NPs were consistently dispersed and confined within a well-defined area, suggesting a well-controlled synthesis process with precise nanoparticle arrangement. Carbon, detected in the mapping, may be originated from the plant extract used in the synthesis process (Fig. 6e). The mapping indicates a reciprocal interaction between ZnO and CuO NPs, indicating their complex spatial distribution. These patterns suggested a close association and provided insight into the cooperative activity occurring during BNP formation.

Identification of bioactive compounds in the *E. foetidum* extract and BNPs by HPLC

HPLC analysis (Fig. 7) was conducted on *E. foetidum* extract before and after the synthesis of BNPs and correlated with the findings from FTIR for the identification of phytocomponents. Various distinct peaks were observed at wavelengths of 270, 280, 310, 320, and 370 nm, each corresponding to specific retention times. The *Eryngium foetidum* extract revealed eight distinct peaks, indicating the presence of various phytocomponents, while the BNPs exhibited a single peak. The retention times of 6.77, 7.53, 15.93, 21.00, 18.90, 28.84, and 30.19 min corresponded

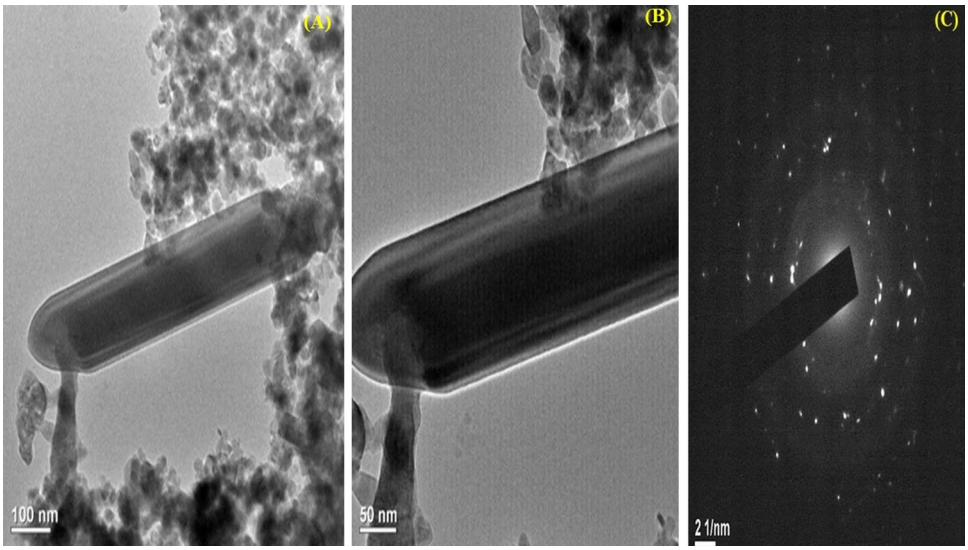

Figure 5. TEM images of *E. foetidum* synthesized CuO–ZnO NPs.

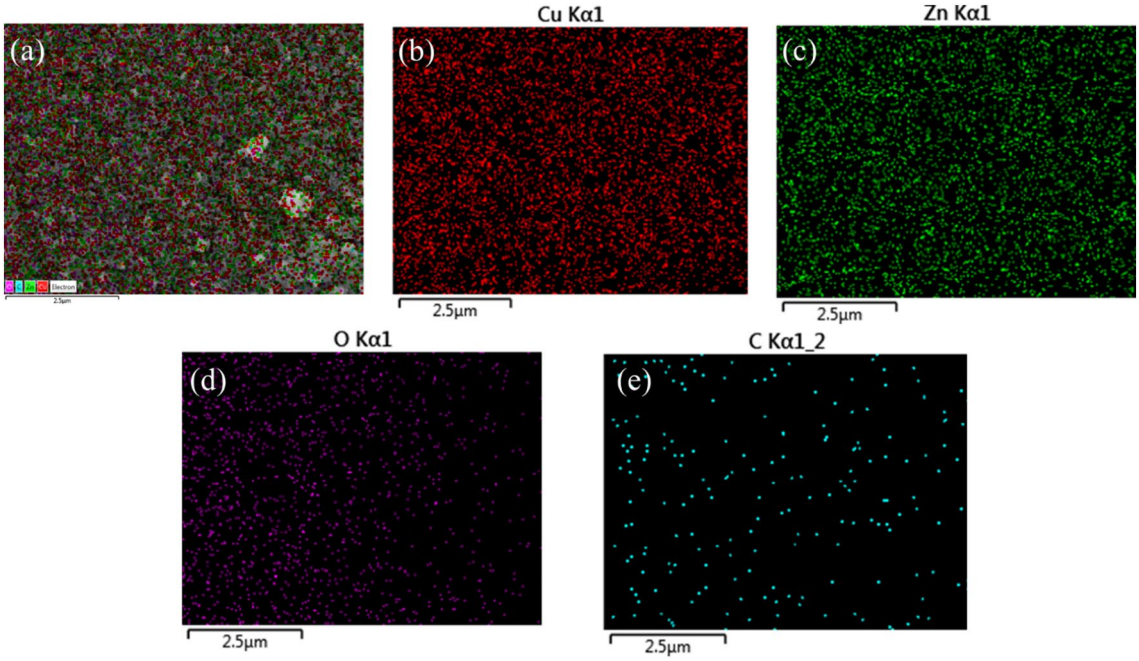

Figure 6. (**a**) Mapping of the CuO–ZnO NPs (**b**) Cu mapping in the NPs (**c**) Zn mapping in the NPs (**d**) O mapping in the NPs (**e**) C mapping in the NPs.

to different phytocomponents, with area percentages of 3.03%, 2.06%, 5.46%, 3.08%, 2.88%, 1.95%, and 2.95% respectively. A retention time of 6.77 (at 326 nm) indicated the presence of phenolic compound, chlorogenic acid which is consistent with previous reports on the *Apiaceae* family to which *E. foetidum* belongs[53]. Similarly, peak at 7.53 (at 326 nm) indicated the presence of carotenoids[54] while peaks at 15.93 and 21.00 suggested the presence of flavone and quercetin, all within the same family of *Apiaceae*[55]. Additionally, retention times of 18.90, 28.84 and 30.19 min corresponded to chlorogenic acid, luteolin hexoside, and luteolin glucuronide, respectively, all belonging to phenolic compounds[56]. Notably, no specific phytocomponents were identified at retention time of 1.92 min (1.54%). The involvement of phytocomponents in capping of nanoparticles during synthesis was further evidenced by the absence of distinct peaks in the HPLC analysis after the synthesis of BNPs, indicated their participation in the synthesis process.

Figure 7A and B illustrates the HPLC chromatogram, demonstrating a noticeable absence of retention time and the phytocomponents originally present in the *E. foetidum* plant after the synthesis of BNPs. Chlorogenic acid, a phenolic compound, was found in the *E. foetidum* plant extract and most abundant polyphehol present in the plant as per previous reports[56]. A possible mechanism for the involvement of most abundant anti-oxidant

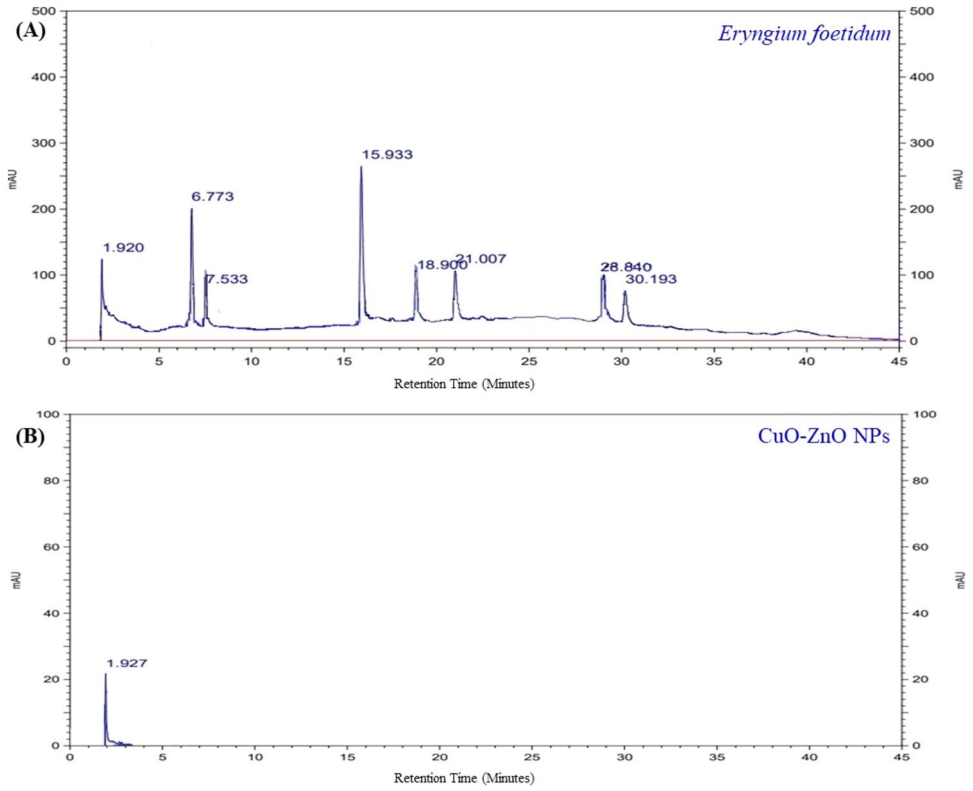

Figure 7. HPLC chromatogram showing the phytocomponents present in (**A**) *Eryngium foetidum* and (**B**) *E. foetidum* synthesized CuO–ZnO NPs.

molecule chlorogenic acid present in *E. foetidum* in the reduction reaction for the formation of CuO–ZnO NPs synthesis is shown in Fig. 8. The hydroxyl groups present in anti-oxidant molecule attacks the metal precursors Cu^{2+} and Zn^{2+} for the formation of BNPs[57]. The other anti-oxidant molecules present in *E. foetidum* extract may also undergo capping reaction with Cu^{2+} and Zn^{2}, which further yield to CuO–ZnO NPs.

We observed from Fig. 2, FTIR peak present in plant extract at 1421 cm^{-1} (responsible for aromatic polyphenols) undergo shift to 1402 cm^{-1} after the formation of BNPs. Similarly, peak shift observed from 1064 cm^{-1} (responsible for C–OH bond stretching in phenols) to 1058 cm^{-1}. The shifting of peaks explains the involvement of polyphenol in NPs formation. The present HPLC analysis provided an additional confirmation of the findings to the FTIR analysis conducted on both the *E. foetidum* plant and the BNPs. HPLC results clearly indicated that the peak at 1.92 was absent in the BNPs synthesis, while all other identified phytocomponents participated in the BNPs formation, confirmed the involvement of polyphenols in the reduction of metal precursors to BNPs.

Applications of CuO–ZnO NPs

Antioxidant activity of CuO–ZnO NPs by DPPH assay

Free radicals are produced in various biological systems, and nanoparticles are commonly employed to eliminate these radicals, which are generated when biomolecules interact with oxygen molecules[58]. The antioxidant activity

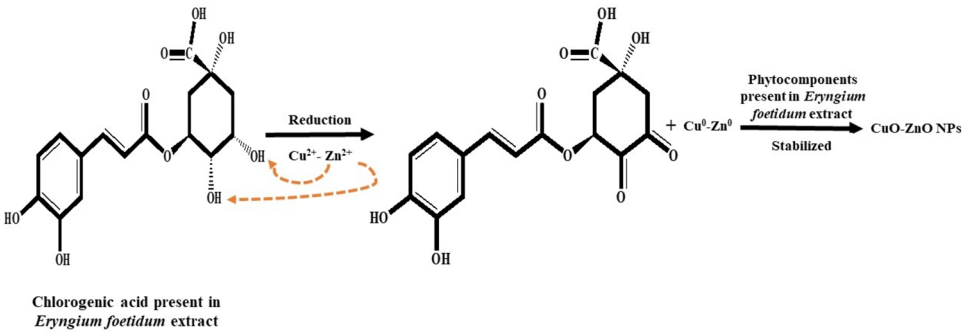

Figure 8. A possible mechanism for the formation of stabilized CuO–ZnO NPs using *E. foetidum* extract.

of biosynthesized BNPs were observed by using the DPPH assay. Figure 9 illustrates the antioxidant activity of BNPs and the standard chlorogenic acid (CGA). The synthesized BNPs demonstrated antioxidant activity by reducing the absorbance against DPPH. The IC_{50} values of the BNPs were compared to the IC_{50} value of CGA. The IC_{50} values of BNPs and CGA observed at 0.253 mg/mL and 0.436 mg/mL, respectively. The antioxidant properties of BNPs were due to different functional groups found in *E. foetidum*. These groups help in the reduction of Cu^{2+}–Zn^{2+} to their metallic forms, Cu^{0}–Zn^{0}, as evidenced by FTIR and confirmed by HPLC data. Previous studies have also shown the antioxidant properties of CuO–ZnO NPs synthesized from various plants such as Neem extract (*Azadirachta indica*), kei apple (*Dovyaliscaffra*), Tulsi extract (*Ocimumtenuiflorum*), and Aloe Vera extract (*Aloe barbadansis*)[22,59].

Antimicrobial activity of CuO–ZnO NPs

Well diffusion method. The antimicrobial activity of BNPs synthesized from *E. foetidum* extract was evaluated using the well diffusion method, demonstrating inhibitory effects against both gram-positive and gram-negative bacterial species: *E. coli*, *E. aerogens*, *S. aureus*, and *B. subtilis*. Gram-positive bacteria like *S. aureus* and *B. subtilis* have a thick peptidoglycan layer surrounding their cells, making them more susceptible to nanoparticle absorption compared to Gram-negative bacteria like *E. coli* and *E. aerogens*, which have thinner cell walls and an additional lipid bilayer membrane. The attachment of nanoparticles to the peptidoglycan layer of Gram-positive bacteria enhances their antimicrobial activity. In contrast, Gram-negative bacteria are more sensitive to the reactive oxygen species (ROS) generated by nanoparticles due to their lipid bilayer membrane, which can disrupt their cellular functions and inhibit their growth[60–62].

The efficiency of these microbes were compared with the standard ampicillin (Table 1). *S. aureus* displayed the greatest activity at 1 mg, 2 mg and 3 mg, with inhibition zones of 17.2 mm, 19.1 mm and 21.1 mm, respectively. Similarly, *E. coli* exhibited the antimicrobial efficacy with a 12.8 mm inhibition zone at 1 mg of BNPs followed by 18.7 mm at 2 mg and 20.7 mm at 3 mg. These findings aligned with prior research indicating significant inhibitory effects of green-synthesized CuO–ZnO nanoparticles on *E. coli* and *S. Aureus*[60]. Additionally, *E. aerogens* and *B. subtilis* demonstrated inhibition zones of 10.1 mm and 10.4 mm at 1 mg, 13.7 mm and 13.4 mm at 2 mg, and 18.7 mm and 15.4 mm at 3 mg, respectively.

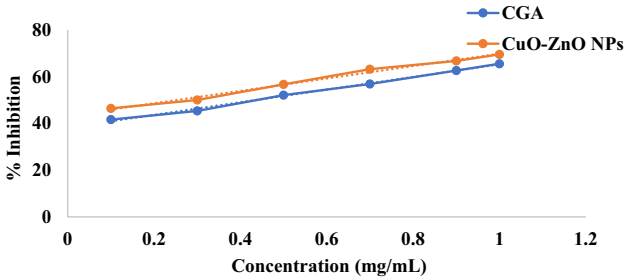

Figure 9. DPPH assay by chlorogenic acid (CGA) and biosynthesized CuO–ZnO NPs using *E. foetidum* extract.

CuO–ZnO NPs (mg/mL)	Microbes	Zone of inhibition (mm)	Efficiency
1 mg	*E. coli*	12.8	+ +
	E. aerogens	10.1	+
	S. aureus	17.2	+ +
	B. subtilis	10.4	+
2 mg	*E. coli*	18.7	+ +
	E. aerogens	13.7	+ +
	S. aureus	19.1	+ +
	B. subtilis	13.4	+ +
3 mg	*E. coli*	20.7	+ +
	E. aerogens	18.7	+ +
	S. aureus	21.1	+ +
	B. subtilis	15.4	+ +
Ampicillin	*E. coli*	30.2	+ + +
	E. aerogens	35.8	+ + +
	S. aureus	38.1	+ + +
	B. subtilis	27.2	+ + +

Table 1. Antimicrobial activity by well diffusion method.

Minimum inhibitory concentration (MIC) of CuO–ZnO NPs. The broth dilution method was utilized to determine the minimum inhibitory concentration (MIC) of the BNPs. This method, includes tube-dilution or macro-broth techniques, which were one of the initial methods used to assess the effectiveness of antimicrobial drugs[62]. MIC is the lowest concentration of BNPs at which there is complete inhibition of microbial growth. The MIC results indicated that BNPs were effective against *S. aureus* at 1 mg, as evidenced by the absence of turbidity (clear solution). For *E. coli*, the effective concentration was 2 mg. Moderate effects were observed against *E. aerogens* and *B. subtilis* at 3 mg (S1). Reportedly, nanocomposites made from Zn-CuO bimetallic nanoparticles have demonstrated significant effectiveness against *E. coli*, *B. subtilis*, and *S. aureus*. The MIC values for these pathogens were 7.81, 62.5, and 31.25 μg mL^{-1}, respectively[63].

Minimum bactericidal concentration (MBC). The MBC test determined the minimum concentration at which BNPs can effectively kill a specific microorganism. MBC studies of BNPs on LB agar plates revealed that at 2 mg, microbial growth was no longer observed for *S. aureus*. Similarly, for *E. coli*, microbial growth ceased at 3 mg. For *E. aerogens* and *B. subtilis*, microbial growth ceased at 4 mg. Thus, the MBC results indicated that BNPs were most effective against *S. aureus*, followed by *E. coli*, with moderate activity against *E. aerogens* and *B. subtilis* (Fig. 10).

The antibacterial mechanism of BNPs were assessed by calculating the ratio of MBC/MIC. MBC/MIC ratio helps to determine bactericidal (killing) or bacteriostatic (growth inhibition) behaviour of anti-microbials[64]. A ratio of MBC/MIC ≤ 2.0 indicates a predominantly bactericidal effect. The BNPs were found to be most bactericidal against *S. aureus*, followed with ratios of ≤ 1.5 for *E. coli*, ≤ 1.33 for *E. aerogens*, and ≤ 1.33 for *B. Subtilis* (S2).

Time kill assay. The Time-Kill Kinetics assay was used to assess the antimicrobial effectiveness of BNPs against different bacterial strains, determining whether the BNPs exhibit bactericidal or bacteriostatic activity over time. At MIC concentrations, incubating the microbes for 24 h resulted in reductions in viable cell counts ranging from 1.344$\log_{10}$ to 3.846$\log_{10}$ CFU/mL for *E. coli*, *E. aerogens*, *S. aureus*, and *B. subtilis*, respectively (Table 2). These reductions indicated significant bactericidal activity. Bactericidal activity was defined as a reduction of 3log10 CFU/mL or more in viable colonies compared to the initial inoculum. BNPs demonstrated effective

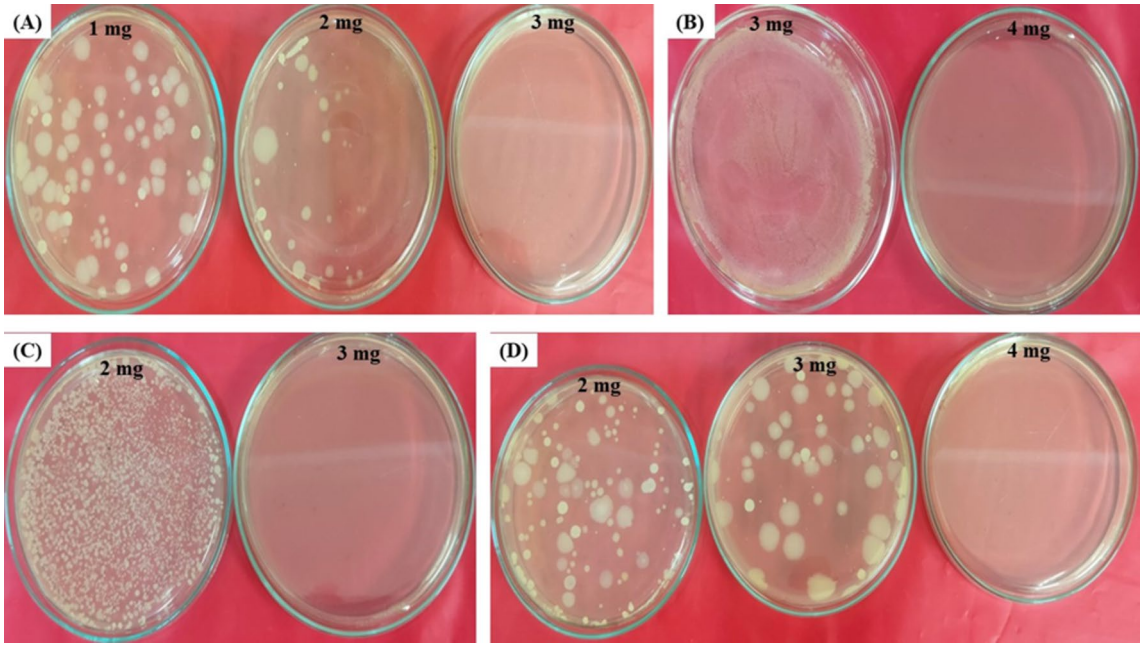

Figure10. Antimicrobial activity shown by the growth of the microbes in LB plates for MBC (**A**) *E. coli,* (**B**) *B. subtilis*, (**C**) *S. aureus,* and (**D**) *E. aerogens.*

Sl. no.	Microbes	MIC	Log_{10} kill at 24 h
1	*E. coli*	2 mg	1.344$\log_{10}$
2	*E.aerogens*	3 mg	0.892$\log_{10}$
3	*S. aureus*	1 mg	3.846$\log_{10}$
4	*B.subtilis*	3 mg	0.416$\log_{10}$

Table 2. Antimicrobial activity shown by time kill assay.

antimicrobial activity against *S. aureus*, followed by *E. coli*, and exhibited moderate effects against *E. aerogens* and *B. subtilis*.

In this antimicrobial investigation, the antimicrobial effectiveness of CuO–ZnO NPs synthesized from *E. foetidum* could be attributed to their impact on cellular metabolism, such as damage to DNA or RNA, disruption of the peptidoglycan layer, rupture of the cell membrane, protein denaturation, or induction of oxidative stress. However, further studies are needed to clarify these mechanisms.

Cytotoxicity studies of CuO–ZnO NPs by MTT assay

The MTT assay is a commonly used colorimetric method to assess cell proliferation and cytotoxicity. It involves the reduction of the yellow MTT dye to formazan crystals. In this study, the MTT assay was used to determine the percentage of viable MCF7 breast cancer cells treated with varying concentrations of BNPs. The concentrations tested were 25, 50, 100, 250, and 500 µg along with untreated MCF7 cells and those treated with 5.75 ± 0.02 mm Cisplatin as a standard (STD) (S3). The results indicated that BNPs exhibited toxicity after 24 h, with an IC_{50} value of 239.99 µg/mL on the MCF7 cell line. The STD treatment resulted in a substantial decrease in cell viability by 31.08%, followed by BNPs at different concentrations: 93.27% for 25 µg, 80.24% for 50 µg, 63.05% for 100 µg, 47.36% for 250 µg, and 39.06% for 500 µg. The assay was conducted in triplicate, and the morphological changes observed are given in Fig. 11. Similar research has been documented involving the creation/synthesis of ZnO-CuO bimetallic nanoparticles through the use of *Artemisia abyssinica* leaf extract. These nanoparticles demonstrated significant toxicity against the MCF-7 cell line, showing a maximum inhibition rate of 89.20 ± 0.03% at a concentration of 500 µg/mL[65].

Discussion

Eryngium foetidum, a commonly found plant used in cooking, was used as the capping and reducing agent in the production of CuO–ZnO nanoparticles. These plant-based extracts have emerged as a simple and environmentally friendly method for synthesizing nanoparticles. It was observed that the BNPs produced had an average size of 16.49 nm and were spherical in shape, as confirmed by TEM analysis. These nanoparticles demonstrated significant therapeutic effects, including antioxidant properties and antimicrobial activity against *E. coli*, *E. aerogens*, *S. aureus*, and *B. subtilis*, as well as anticancer effects against MCF7 cells (breast cancer). Therefore, with further clinical trials and *in-vivo* studies, the nanoparticles synthesized in this manner could potentially be developed into drugs/ nanomedicines.

The formation of rod-shaped CuO–ZnO NPs were confirmed by UV–Vis, XRD, FESEM, TEM. The purity of the biosynthesized BNPs was analysed by EDX analysis. The anti-oxidant activity of CuO–ZnO NPs found was 0. 253 mg/mL. The observed anti-microbial activity of BNPs with the help of disk diffusion method, MIC method, MBC method and time kill method was observed that the anti-microbial efficacy of CuO–ZnO NPs followed an increasing order: *B. subtilis* < *E. aerogens* < *E. coli* < *S. aureus*.

Significant cytotoxic activity against MCF7 breast cancer cell lines was also noticed within IC_{50} 239.99 µg/mL. From Table 3, it was observed that the difference between the recent research and the present study. The IC_{50} of antioxidant activity was reported to be 253 µg/mL which was almost equivalent to previous reports with the IC_{50}

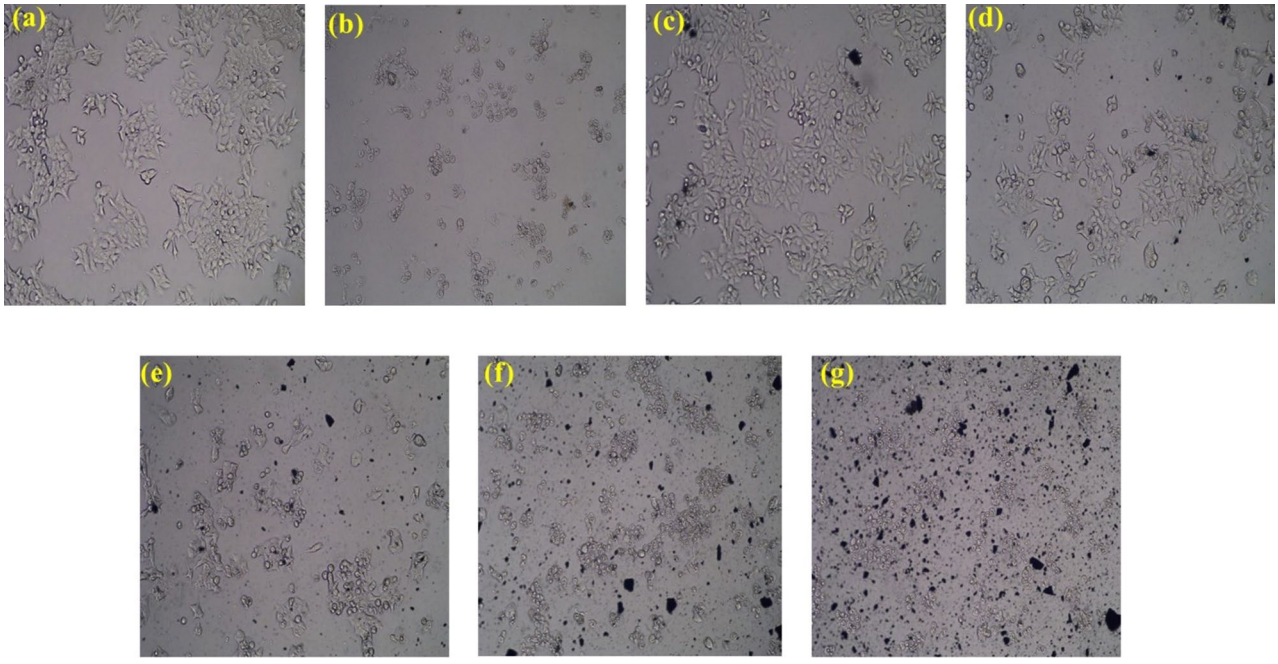

Figure 11. Morphology of MCF7 cell untreated (**a**), standard (STD) (**b**), 25 µg/mL (**c**), 50 µg/mL (**d**), 100 µg/mL (**e**), 250 µg/mL (**f**) and 500 µg/mL (**g**).

Biological analysis	Ratios of CuO–ZnO NPs	Results	Ref
Antioxidant	1:1	IC_{50} = 253 µg/mL	Present study
	1:1	IC_{50} = 3.28 µg/mL	[65]
	1:5	IC_{50} = 3.92 mg/mL	[22]
	7:3, 1:1 and 3:7	IC_{50} = 217.82, 236.41 and 263.72 µg/mL	[66]
	1:1	IC_{50} = 68.28 µg/mL	[67]
Antimicrobial	1:1	*S. aureus* > *E. coli* > *E. aerogens* > *B. subtilis*	Present study
	1:1	*B. subtilis* > *S. aureus* > *E. coli* > *P. aeruginosa*	[66]
	1:1	*E. coli* > *P. aeruginosa* > *S. aureus*	[67]
	1:1	*S. mutans* > *A. baumannii* > *B. cereus* > *S. aureus* > *K. pneumoniae*	[68]
Anticancer (MCF-7 cell)	1:1	IC_{50} = 239.99 µg/mL	Present study
	1:1	IC_{50} = 247.15 µg/mL	[65]
	1:2	IC_{50} = 25 µg/mL	[40]
	1:5	IC_{50} = 3.87 µg/mL	[22]

Table 3. Comparison of biological analyses with those in previously published reports.

of 236.41 µg/mL in the 1:1 ratio[67]. Depending on the ratios of the metal and the extracts used; the results showed the anti-oxidant capacity of the synthesized BNPs. Similarly, antimicrobial studies showed that *S. aureus* is highly inhibited followed by *E. coli, E. aerogens* and *B. Subtilis* microbes. Furthermore, anticancer studies showed better activity with the IC_{50} of 239.99 µg/mL than the earlier reports with IC_{50} of 247.15 µg/mL but lower activities with IC_{50} = 25 µg/mL and with IC_{50} = 3.87 µg/mL which might be due to the higher ratio of the metal[22,44,66].

Conclusion

This present study demonstrated that the leaf extract of the medicinal plant *E. foetidum* was effectively used to synthesize CuO–ZnO NPs using a low-cost, efficient and simple method. TEM analysis revealed that the nanoparticles had an average size of 16 nm. FTIR analysis suggested that polyphenols, carbohydrates, flavonoids, and other phytocomponents acted as stabilizing and capping agents during the synthesis of the nanoparticles. XRD confirmed the crystalline structure of the nanoparticles, with sizes ranging from 7 to 23 nm. HPLC studies identified seven phytocomponents that contributed to bio-reduction. Although, slight toxicity of CuO NPs as anti-cancer drug is a little matter of concern but using in combinations with ZnO beneficial effects are observed[16]. CuO–ZnO BNPs exhibited significant toxicity against MCF-7 cancer cells, with an IC_{50} value of 239.99 µg/mL, and demonstrated strong antioxidant activity, with an IC_{50} value of 0.253 mg/mL. Additionally, the BNPs showed the highest antimicrobial activity against *S. aureus* and the lowest against *B. subtilis*.

Data availability

All raw data related to the experimental results are submitted as supplementary data.

Received: 16 May 2024; Accepted: 9 August 2024
Published online: 22 August 2024

References

1. Muthuvel, A., Jothibas, M., Manoharan, C. & Jayakumar, S. J. Synthesis of CeO 2-NPs by chemical and biological methods and their photocatalytic, antibacterial and in vitro antioxidant activity. *Res. Chem. Inter.* **46**, 2705–2729 (2020).
2. Muthuvel, A., Jothibas, M., Mohana, V. & Manoharan, C. Green synthesis of cerium oxide nanoparticles using *Calotropis procera* flower extract and their photocatalytic degradation and antibacterial activity. *Inorg. Chem. Commun.* **119**, 108086 (2020).
3. Stamenkovic, V. Platinum in fuel cells gets a helping hand. *Science* **5809**, 172 (2007).
4. Elemike, E. E., Onwudiwe, D. C., Nundkuma, R. N., Singh, M. & Iyekowa, O. Green synthesis of Ag, Au and Ag-Au bimetallic nanoparticles using *Stigmaphyllon ovatum* leaf extract and their in vitro anticancer potential. *Mater. Lett.* **243**, 148–152 (2019).
5. Ramesh, M., Anbuvannan, M. & Viruthagiri, G. Green synthesis of ZnO nanoparticles using Solanum nigrum leaf extract and their antibacterial activity. *Spectrochim. Acta Part A Mol. Biomol. Spect.* **136**, 864–870 (2015).
6. Akintelu, S. A., Folorunso, A. S., Folorunso, F. A. & Oyebamiji, A. K. Green synthesis of copper oxide nanoparticles for biomedical application and environmental remediation. *Heliyon* **6**, e04508 (2020).
7. Ealia, S. A. M. & Saravanakumar, M. P. A review on the classification, characterisation, synthesis of nanoparticles and their application. In *IOP Conference Series: Materials Science and Engineering.* Preprint at https://doi.org/10.1088/1757-899X/263/3/032019 (IOP Publishing, 2017).
8. Hasan, S. A review on nanoparticles: Their synthesis and types. *Res. J. Recent Sci.* **4**, 911 (2015).
9. Muthuvel, A., Said, N. M., Jothibas, M., Gurushankar, K. & Mohana, V. Microwave-assisted green synthesis of nanoscaled titanium oxide: Photocatalyst, antibacterial and antioxidant properties. *J. Mater. Sci. Mater. Electron.* **32**, 23522–23539 (2021).
10. Arumugam, A. *et al.* Synthesis of cerium oxide nanoparticles using *Gloriosa superba* L. leaf extract and their structural, optical and antibacterial properties. *Mater. Sci. Eng. C.* **49**, 408–415 (2015).
11. Al-Zaqri, N., Umamakeshvari, K., Mohana, V., Muthuvel, A. & Boshaala, A. Green synthesis of nickel oxide nanoparticles and its photocatalytic degradation and antibacterial activity. *J. Mater. Sci. Mater. Electron.* **33**, 11864–11880 (2022).
12. Velsankar, K., Sudhahar, S., Parvathy, G. & Kaliammal, R. Effect of cytotoxicity and a antibacterial activity of biosynthesis of ZnO hexagonal shaped nanoparticles by *Echinochloa frumentacea* grains extract as a reducing agent. *Mater. Chem. Phys.* **239**, 121976 (2020).
13. Velsankar, K., Sudhahar, S. & Maheshwaran, G. Effect of biosynthesis of ZnO nanoparticles via Cucurbita seed extract on *Culex tritaeniorhynchus* mosquito larvae with its biological applications. *J. Photochem. Photobiol. B Biol.* **200**, 111650 (2019).

14. Velsankar, K., Parvathy, G., Mohandoss, S. & Sudhahar, S. Effect of green synthesized ZnO nanoparticles using *Paspalum scrobiculatum* grains extract in biological applications. *Microsc. Res. Tech.* **85**, 3069–3094 (2022).
15. Velsankar, K. *et al.* Green inspired synthesis of ZnO nanoparticles and its characterizations with biofilm, antioxidant, anti-inflammatory, and anti-diabetic activities. *J. Mol. Struct.* **1255**, 132420 (2022).
16. Grigore, M. E., Biscu, E. R., Holban, A. M., Gestal, M. C. & Grumezescu, A. M. Methods of synthesis, properties and biomedical applications of CuO nanoparticles. *Pharmaceuticals* **9**, 75 (2016).
17. Velsankar, K., Vinothini, V., Sudhahar, S., Kumar, M. K. & Mohadoss, S. Green synthesis of CuO nanoparticles via *Plectranthus amboinicus* leaves extract with its characterization on structural, morphological, and biological properties. *Appl. Nanosci.* **10**, 3953–3971 (2020).
18. Velsankar, K., Parvathy, G., Mohandoss, S., Kumar, R. M. & Sudhahar, S. Green synthesis and characterization of CuO nanoparticles using *Panicum sumatrense* grains extract for biological applications. *Appl. Nanosci.* **12**, 1993–2021 (2022).
19. Velsankar, K., Aravinth, K., Yong, W., Mohandoss, S. & Paiva-Santos, A. C. NiO nanoparticles, an algorithm of their biosynthesis, toxicity, and biomedical activities. *J. Mol. Struct.* **1291**, 136012 (2023).
20. Velsankar, K., Suganya, S., Muthumari, P., Mohandoss, S. & Sudhahar, S. Ecofriendly green synthesis, characterization and biomedical applications of CuO nanoparticles synthesized using leaf extract of *Capsicum frutescens*. *J. Environ. Chem. Eng.* **9**, 106299 (2021).
21. Jiang, J., Pi, J. & Cai, J. The advancing of zinc oxide nanoparticles for biomedical applications. *Bioinorg. Chem. Appl.* **2018**, 1062562 (2018).
22. Adeyemi, J. O., Onwudiwe, D. C. & Oyedeji, A. O. Biogenic synthesis of CuO, ZnO, and CuO–ZnO nanoparticles using leaf extracts of *Dovyalis caffra* and their biological properties. *Molecules* **27**, 3206 (2022).
23. Paul, J. H., Seaforth, C. E. & Tikasingh, T. *Eryngium foetidum* L.: A review. *Fitoterapia* **82**, 302–308 (2011).
24. Chowdhury, J. U., Nandi, N. C. & Yusuf, M. Chemical constituents of essential oil of the leaves of *Eryngium foetidum* from Bangladesh. *Bangladesh J. Sci. Ind. Res.* **42**, 347–352 (2007).
25. Rodrigues, T. L., Silva, M. E., Gurgel, E. S., Oliveira, M. S. & Lucas, F. C. *Eryngium foetidum* L. (Apiaceae): A literature review of traditional uses, chemical composition, and pharmacological activities. *Evid.-Based Complement. Altern. Med.* **2022**, 2896895 (2022).
26. Bray, F. *et al.* Global cancer statistics 2018: GLOBOCAN estimates of incidence and mortality worldwide for 36 cancers in 185 countries. *CA Cancer J. Clin.* **68**, 394–424 (2018).
27. Gardea-Torresdey, J. L. *et al.* Formation and growth of Au nanoparticles inside live alfalfa plants. *Nano Lett.* **2**, 397–401 (2002).
28. Zhang, H., Li, T., Luo, W., Peng, G. X. & Xiong, J. Green synthesis of Ag nanoparticles from *Leucus aspera* and its application in anticancer activity against alveolar cancer. *J. Exp. Nanosci.* **17**, 47–60 (2022).
29. Flieger, J., Flieger, W., Baj, J. & Maciejewski, R. Antioxidants: Classification, natural sources, activity/capacity measurements, and usefulness for the synthesis of nanoparticles. *Mater.* **14**, 4135 (2021).
30. Ng, M. L. *et al.* Role of reactive oxygen species (ROS) in aging and aging-related diseases. *Res. J. Pharm. Bio. Chem. Sci.* **9**, 44–51 (2018).
31. Rodrigo, R. *Oxidative Stress and Antioxidants: Their Role in Human Disease* 1–358 (Nova Biomedical Books, 2009).
32. Munteanu, I. G. & Apetrei, C. Analytical methods used in determining antioxidant activity: A review. *Int. J. Mol. Sci.* **22**, 3380 (2021).
33. Shahidi, F. & Zhong, Y. Measurement of antioxidant activity. *J. Funct. Foods* **18**, 757–781 (2015).
34. Wang, L., Hu, C. & Shao, L. The antimicrobial activity of nanoparticles: Present situation and prospects for the future. *Int. J. Nanomed.* **12**, 1227–1249 (2017).
35. Naikoo, G. A. *et al.* Bioinspired and green synthesis of nanoparticles from plant extracts with antiviral and antimicrobial properties: A critical review. *J. Saudi Chem. Soc.* **25**, 101304 (2021).
36. Dadi, R., Azouani, R., Traore, M., Mielcarek, C. & Kanaev, A. Antibacterial activity of ZnO and CuO nanoparticles against gram positive and gram negative strains. *Mater. Sci. Eng. -C* **104**, 109968 (2019).
37. Anjum, S., Nawaz, K., Ahmad, B., Hano, C. & Abbasi, B. H. Green synthesis of biocompatible core–shell (Au–Ag) and hybrid (Au–ZnO and Ag–ZnO) bimetallic nanoparticles and evaluation of their potential antibacterial, antidiabetic, antiglycation and anticancer activities. *RSC Adv.* **12**, 23845–23859 (2022).
38. Sindhudevi, M., Srinivasan, S., Karthekiyan, B. & Muthuvel, A. Green synthesis and characterization of Selenium/Zirconium bimetallic nanoparticles using *Cinnamomum camphora* leaf extract and their photocatalyst and anticancer activity. *J. Water Environ. Nanotech.* **8**, 417–441 (2023).
39. Cao, Y. *et al.* Green synthesis of bimetallic ZnO–CuO nanoparticles and their cytotoxicity properties. *Sci. Rep.* **11**, 23479 (2021).
40. Madeshwaran, K. & Venkatachalam, R. Green synthesis of bimetallic ZnO–CuO nanoparticles using *Annona muricata* l. extract: Investigation of antimicrobial, antioxidant, and anticancer properties. *J. Ind. Eng. Chem.* https://doi.org/10.1016/j.jiec.2024.06.002 (2024).
41. Alley, M. *et al.* Validation of an automated microculture tetrazolium assay (MTA) to assess growth and drug sensitivity of human tumor cell lines. *Int. Proc. Am. Assoc. Cancer Res.* **27**, 389–389 (1986).
42. Mosmann, T. Rapid colorimetric assay for cellular growth and survival: Application to proliferation and cytotoxicity assays. *J. Immunol. Methods* **65**, 55–63 (1983).
43. Gosens, I. *et al.* Impact of agglomeration state of nano- and submicron sized gold particles on pulmonary inflammation. *Particle Fibre Toxicol.* **7**, 37 (2010).
44. Grasel, F. D. S., Ferrão, M. F. & Wolf, C. R. Development of methodology for identification the nature of the polyphenolic extracts by FTIR associated with multivariate analysis. *Spectrochim. Acta Part A Mol. Biomol. Spectrosc.* **153**, 94–101 (2016).
45. Ernawita, *et al.* In vitro lipophilic antioxidant capacity, antidiabetic and antibacterial activity of citrus fruits extracts from Aceh, Indonesia. *Antioxidants* **6**, 11 (2017).
46. Zannini, D., Dal, P. G., Malinconico, M., Santagata, G. & Immirzi, B. Citrus pomace biomass as a source of pectin and lignocellulose fibers: From waste to upgraded biocomposites for mulching applications. *Polymers* **13**, 1280 (2021).
47. Ajuong, E. & Birkinshaw, C. The effects of acetylation on the extractives of Sitka Spruce (*Picea sitchensis*) and Larch (*Larix leptoleptis*) wood. *Eur. J. Wood Wood Prod.* **62**, 189–196 (2004).
48. Chien, W.-J., Saputri, D. S. & Lin, H.-Y. Valorization of Taiwan's *Citrus depressa* Hayata peels as a source of nobiletin and tangeretin using simple ultrasonic-assisted extraction. *Curr. Res. Food Sci.* **5**, 278–287 (2022).
49. Kumar, K. J., Basumatary, S., Daimari, J., Mondal, A. & Deka, A. K. Photocatalytic degradation of methylene blue with polyphenol rich *Citrus limetta* (peel waste) facilitated ZnO nanoparticles under sunlight. *React. Kinet. Mech. Cat.* **137**, 483–503 (2024).
50. Iravani, S. Green synthesis of metal nanoparticles using plants. *Green Chem.* **13**, 2638–2650 (2011).
51. Fang, J. & Xuan, Y. Investigation of optical absorption and photothermal conversion characteristics of binary CuO/ZnO nanofluids. *RSC Adv.* **7**, 56023–56033 (2017).
52. Wasim, M. *et al.* Surface modification of bacterial cellulose by copper and zinc oxide sputter coating for UV-resistance/antistatic/antibacterial characteristics. *Coatings* **10**, 364 (2020).
53. Ayuso, M. *et al.* Phenolic composition and biological activities of the in vitro cultured endangered *Eryngium viviparum*. *J. Gay. Ind. Crops Prod.* **148**, 112325 (2020).

54. Leitão, D. D. S. T. C. *et al.* Amazonian *Eryngium foetidum* leaves exhibited very high contents of bioactive compounds and high singlet oxygen quenching capacity. *Int. J. Food Prop.* **23**, 1452–1464 (2020).
55. Derda, M., Thiem, B., Budzianowski, J., Wojt, W. J. & Wojtkowiak-Giera, A. The evaluation of the amebicidal activity of *Eryngium planum* extracts. *Acta Poloniae Pharmaceutica* **70**, 1027–1034 (2013).
56. Leitão, D. D. S. T. C. Extracts of *Eryngium foetidum* leaves from the Amazonia were efficient scavengers of ROS and RNS. *Antioxidants* **12**, 1112 (2023).
57. Naseer, M., Aslam, U., Khalid, B. & Chen, B. Green route to synthesize zinc oxide nanoparticles using leaf extracts of *Cassia fistula* and *Melia azadarach* and their antibacterial potential. *Sci. Rep.* **10**, 9055 (2020).
58. Muthuvel, A., Jothibas, M. & Manoharan, C. Synthesis of copper oxide nanoparticles by chemical and biogenic methods: Photocatalytic degradation and in vitro antioxidant activity. *Nanotech. Environ. Eng.* **5**, 14 (2020).
59. Vibitha, B. V., Anitha, B., Krishna, P. G. A. & Tharayil, J. N. Plant extracts assisted synthesis, characterization and antioxidant properties of ZnO: CuO nanocomposites. *AIP Conf. Proc.* https://doi.org/10.1063/5.0009174 (2020).
60. Takele, E., Feyisa, B. R., Shumi, G. & Kenasa, G. Green synthesis, characterization, and antibacterial activity of CuO/ZnO nanocomposite using *Zingiber officinale* rhizome extract. *J. Chem.* **2023**, 3481389 (2023).
61. Dutta, R. K., Sharma, P. K., Bhargava, R., Kumar, N. & Pandey, A. C. Differential susceptibility of *Escherichia coli* cells toward transition metal-doped and matrix-embedded ZnO nanoparticles. *J. Phys. Chem. B* **114**, 5594–5599 (2010).
62. Verma, A. & Balekar, N. Antimicrobial susceptibility testing: A comprehensive review. *Int. J. Newgen Res. Pharm. Healthc.* **2023**, 08–14 (2023).
63. Hasanin, M. S., Hashem, A. H., Al-Askar, A. A., Haponiuk, J. & Saied, E. A novel nanocomposite based on mycosynthesized bimetallic zinc-copperoxide nanoparticles, nanocellulose and chitosan: Characterization, antimicrobial and photocatalytic activities. *Electron. J. Biotechnol.* **65**, 45–55 (2023).
64. Huang, X. J. *et al.* The antibacterial properties of 4, 8, 4′, 8′-tetramethoxy (1,1′-biphenanthrene)-2,7,2′,7′-tetrol from fibrous roots of *Bletilla striata*. *Indian J. Microbiol.* **61**, 195–202 (2021).
65. Orshiso, T. A. *et al.* Biosynthesis of *Artemisia abyssinica* leaf extract-mediated bimetallic ZnO–CuO nanoparticles: Antioxidant, anticancer, and molecular docking studies. *ACS Omega* **8**, 41039–41053 (2023).
66. Nguyen, T. T. T., Nguyen, Y. N. N., Tran, X. T., Nguyen, T. T. T. & Van, T. T. Green synthesis of CuO, ZnO and CuO/ZnO nanoparticles using *Annona glabra* leaf extract for antioxidant, antibacterial and photocatalytic activities. *J. Environ. Chem. Eng.* **11**, 111003 (2023).
67. Dubey, S., Shukla, A. & Shukla, R. Green synthesis, characterization, and biological activities of Zn, Cu monometallic and bimetallic nanoparticles using *Borassus flabellifer* leaves extract. *Curr. Chem. Lett.* **12**, 799–812 (2023).
68. Fathima, F. P. *et al.* Green synthesis of CuO/ZnO nanocomposites using *Ficus drupacea*: In-vitro antibacterial and cytotoxicity analysis. *ChemistrySelect* **9**, e202401235 (2024).

Acknowledgements

We express our gratitude to the Institute of Advanced Study in Science and Technology, (Assam, India) for supplying XRD and FESEM data for our analysis. We also acknowledge the CIF at Lovely Professional University (Punjab, India) for conducting Elemental mapping analysis. We appreciate Dr. Sourav Dey from Guwahati Biotech Park (Assam, India) for performing HPLC analysis and SAIF, North-Eastern Hill University (Meghalaya, India) for providing TEM data. Special thanks are extended to Stellixir Biotech Pvt. Ltd., (Bangalore, India) a specialized provider of preclinical and R&D services for antimicrobial and anticancer studies.

Author contributions

Jennifer Daimari: Data evaluation, writing of manuscript. Anamika Kalita Deka: Conceptualisation, supervise, editing and re writing the manuscript.

Funding

This work was supported by the University Grants Commission, New Delhi, for the award of NFST research fellowship with the award number 202122-NFST-ASS-00285 to J. Daimari.

Competing interests

The authors declare no competing interests.

Additional information

Supplementary Information The online version contains supplementary material available at https://doi.org/10.1038/s41598-024-69847-w.

Correspondence and requests for materials should be addressed to A.K.D.